Editors' Suggestion

Benefit from Photon Recycling at the Maximum-Power Point of State-of-the-Art Perovskite Solar Cells

Roberto Brenes,[1,2,‡] Madeleine Laitz,[1,2,‡] Joel Jean,[1,3] Dane W. deQuilettes,[2,*] and Vladimir Bulović[1,2,†]

[1] *Department of Electrical Engineering and Computer Science, Massachusetts Institute of Technology, 77 Massachusetts Avenue, Cambridge, Massachusetts 02139, USA*

[2] *Research Laboratory of Electronics, Massachusetts Institute of Technology, 77 Massachusetts Avenue, Cambridge, Massachusetts 02139, USA*

[3] *Swift Solar Inc., Golden, Colorado 80401, USA*

(Received 4 February 2019; revised manuscript received 29 April 2019; published 10 July 2019)

Photon recycling is required for a solar cell to achieve an open-circuit voltage (V_{OC}) and power conversion efficiency (PCE) approaching the Shockley-Queisser theoretical limit. The achievable performance gains from photon recycling in metal halide perovskite solar cells remain uncertain due to high variability in material quality and the nonradiative recombination rate. We quantify the enhancement due to photon recycling for state-of-the-art perovskite $Cs_{0.05}(MA_{0.17}FA_{0.83})_{0.95}Pb(I_{0.83}Br_{0.17})_3$ (triple-cation) films and corresponding solar cells. We show that, at the maximum power point (MPP), the absolute PCE can increase up to 2.0% in the radiative limit, primarily due to a 77 mV increase in (V_{MPP}). For this photoactive layer, even with finite nonradiative recombination, benefits from photon recycling can be achieved when nonradiative lifetimes and external light-emitting diode (LED) electroluminescence efficiencies, Q_e^{LED}, exceed 2 μs and 10%, respectively. This analysis quantifies the significance of photon recycling in boosting the real-world performance of perovskite solar cells toward theoretical limits.

DOI: 10.1103/PhysRevApplied.12.014017

I. INTRODUCTION

Improving solar cell power conversion efficiency (PCE) requires both optimization of device architectures and an understanding of fundamental photophysics. For example, PCEs of GaAs cells increased from 25.1% to 28.8% through photon management [1–4]. In luminescent optoelectronic materials, such as GaAs, photons can undergo multiple absorption and emission events before escaping, a phenomenon called photon recycling. During steady-state operation, photon recycling increases the charge carrier density within the photoactive cell layers, resulting in a higher quasi-Fermi level energy splitting (μ) and increased open-circuit voltage (V_{OC}) through $\mu = qV_{OC}$ [4–7]. Photon recycling also slows the external photon emission rate, decreasing the radiative saturation current [8,9]. Together, these effects can boost the performance of high-efficiency solar cells toward the Shockley-Queisser theoretical limit. To take advantage of photon recycling, a photovoltaic (PV) absorber material must exhibit a small Stokes shift, strong band-edge absorption, and high photoluminescence quantum efficiency (PLQE) [3–5,10–12].

Relatively low PLQEs have thus far limited the extent of photon recycling observed in perovskite thin films and single crystals [13–15]. Low PLQEs of <15% result from high first-order nonradiative recombination rates, (k_1) on the order of 10^6–10^9 s^{-1}, which are associated with trap state densities of 10^{15}–10^{17} cm^{-3} [16–18]. For example, Pazos-Outón *et al.* demonstrated that the average photon only undergoes one recycling event in a typical $CH_3NH_3PbI_3$ film, but predicted that up to 25 recycling events could be sustained with a sufficiently high-quality sample [13]. This is in contrast to GaAs films used in state-of-the-art PV devices, where an average photon can participate in up to 50 recycling events [3]. In thick perovskite single crystals, several reports have used time-resolved photoluminescence spectroscopy to show a characteristic redshift in emission spectra over time due to photon recycling [13]. This phenomenon is expected to be efficient in single crystals, which exhibit low bulk defect densities (approximately 10^{10} cm^{-3}). However, the high surface recombination velocities of 5800 cm s^{-1} lead to rapid quenching of excess carriers, diminishing the probability of photon recycling [14,19–23].

Passivated perovskite thin films with record-low nonradiative recombination rates and defect densities have achieved internal PLQEs exceeding 90% [18,24,25]—approaching the highest-quality double-

*danedeq@mit.edu
†bulovic@mit.edu
‡These authors contributed equally to this work.

heterostructured GaAs films [26]. These recent advances in material quality should enable improved photon recycling and light management in perovskite devices, but thus far, it has been unclear how to realize practical efficiency gains. Futhermore, other works have only considered the impact of photon recycling on perovskite solar cells at open circuit, where the extent of recycling differs significantly from operation at the maximum power point (MPP). Under operation, rapid charge extraction reduces the steady-state carrier density, allowing nonradiative processes to compete with radiative recombination and photon recycling. The practical importance of photon recycling in perovskite solar cells thus remains unclear.

Here, we perform a theoretical analysis of photon recycling in state-of-the-art $Cs_{0.05}(MA_{0.17}FA_{0.83})_{0.95}Pb(I_{0.83}Br_{0.17})_3$ (triple-cation) films, which, in PV devices, have demonstrated record efficiencies and high stability [27,28]. We examine the impact of photon recycling at the MPP with varying first-order nonradiative recombination rates and external emission efficiencies [29,30]. The analysis is extended to $CH_3NH_3PbI_3$ films, which have been extensively studied previously, serving as a benchmark to compare emerging perovskite formulations (see Supplemental Material Figs. S21–S28 [31]). Our model reveals the changes in carrier density and luminescence efficiency at MPP attributable to photon recycling and identifies optoelectronic material quality targets—that is, external luminescence quantum efficiency and nonradiative recombination rates—toward which the community can strive. Quantifying these values is critical, as several reports have shown that devices with low nonradiative recombination can achieve V_{OC} deficits below 0.4 V, which is the deficit regime in which GaAs solar cells began to benefit from photon recycling [2,32–36].

II. PHOTON RECYCLING IN THE DETAILED BALANCE MODEL

A. Radiative limit

To quantify the effect of photon recycling on device performance, current-voltage (J-V) curves are simulated using a detailed balance model and experimentally determined absorption coefficient and refractive index data for $Cs_{0.05}(MA_{0.17}FA_{0.83})_{0.95}Pb(I_{0.83}Br_{0.17})_3$ (see Fig. S8 within the Supplemental Material [31]) [16,29]. In the Supplemental Material, we discuss key assumptions used in the model, which are consistent with previous analyses [7,13,29,31,37–39].

We first perform a detailed balance calculation in the radiative limit (i.e., no nonradiative recombination, $k_1 = 0$) by equating the generation current with the recombination and extraction currents. The total current (J_{total}) as a function of voltage (V) is then defined as

$$J_{\text{total}}(V) = J_{SC} - J_0^{\text{rad,ext}}(V), \tag{1}$$

where J_{SC} is the short-circuit current density

$$J_{\text{SC}} = q\int_0^{\infty} a(E)\phi_{\text{sun}}(E)dE, \tag{2}$$

and $J_0^{\text{rad,ext}}$ is the external radiative saturation current, defined as the photon flux that escapes the film into the surrounding atmosphere multiplied by the fundamental charge, q,

$$J_0^{\text{rad,ext}}(V) = q\pi e^{qV/kT}\int_0^{\infty} a(E)\phi_{\text{BB}}(E)dE, \tag{3}$$

where k is the Boltzmann constant, T is the cell temperature, $a(E)$ is the absorptivity $\{a(E) = 1 - \exp[-2\cdot\alpha(E)\cdot d]\}$ as previously defined elsewhere [3,40], d is the film thickness ($d = 500$ nm), $\alpha(E)$ is the energy-dependent absorption coefficient, $\phi_{\text{sun}}(E)$ is the AM1.5 spectral photon flux, and $\phi_{\text{BB}}(E)$ is the blackbody spectral photon flux all as a function of energy, E.

Importantly, and as discussed in depth previously [38,39], photon recycling is implicit in the Shockley-Queisser detailed balance calculation, where the total photon flux emitted from the front surface of the device is used to determine the external radiative saturation current: $J_0^{\text{rad,ext}}$ [Eq. (3)]. Here, only the emitted photons in the escape cone contribute to $J_0^{\text{rad,ext}}$, regardless of the number of photon recycling events before escape (see Supplemental Material for discussion of the escape cone [31]) [37,41].

Next, we determine the benefits of photon recycling by considering the radiative saturation current when photon recycling is not included in the calculation [37,42]. The internal radiative saturation current ($J_0^{\text{rad,int}}$) is similar to the external radiative saturation current, but is enhanced by the photon mode density within the photoactive dielectric medium characterized by the index of refraction, $n_r(E)$, absorption coefficient, and integrated over the sphere of emission [38]. Equation (4) describes a microscopic view of recombination within the active region where all photons immediately escape into the surrounding environment [37,41]

$$J_0^{\text{rad,int}}(V) = qe^{qV/kT}\int_0^{\infty} 4\pi n_r^2(E)\alpha(E)\phi_{\text{BB}}(E)dE. \tag{4}$$

We use $J_0^{\text{rad,int}}$ to calculate the intrinsic carrier density [van Roosebroeck-Shockley relationship, Eq. (5)] from standard reported second-order internal radiative recombination rate constants (k_2^{int}) for triple-cation films, $k_2^{\text{int}} = 2\times10^{-10}\,\text{cm}^{-3}\,\text{s}^{-1}$ [17,29,43]. The radiative recombination rate constant is an intrinsic material property for a

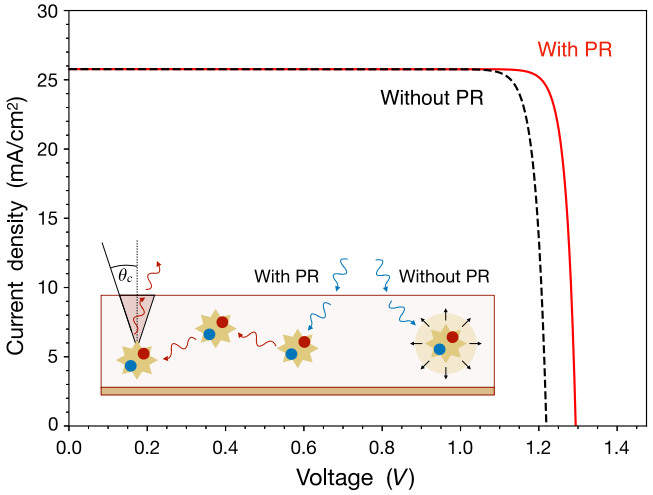

FIG. 1. Detailed-balance simulation of *J-V* curves for an ideal $Cs_{0.05}(MA_{0.17}FA_{0.83})_{0.95}Pb(I_{0.83}Br_{0.17})_3$ perovskite photovoltaic device in the radiative limit (no nonradiative recombination) with (red trace) and without (black dashed trace) photon recycling (PR).

given perovskite film composition and is not varied in this analysis. We find the external radiative recombination rate constant (k_2^{ext}) and intrinsic carrier density to be $k_2^{\text{ext}} = 1 \times 10^{-11}\ \text{cm}^{-3}\,\text{s}^{-1}$ and $n_i = 2.3 \times 10^5\ \text{cm}^{-3}$, respectively (see Supplemental Material for the determination of k_2^{ext} and n_i [31]), which agree with experimental reports considering photon recycling effects [17,24,43–45].

$$k_2^{\text{int}} n_i^2 = \int_0^\infty 4\pi n_r^2(E)\alpha(E)\Phi_{\text{BB}}(E)dE. \tag{5}$$

In order to make our calculations relevant for real-world perovskite devices exhibiting band tailing likely due to disorder [46,47], we experimentally determine the energy-dependent absorption coefficient and refractive index using photothermal deflection spectroscopy and ellipsometry (see Figs. S8 and S19 within the Supplemental Material [31]). Figure 1 shows the theoretical current-voltage (*J-V*) curves for a triple-cation perovskite solar cell (see Supplemental Material for equivalent curves with $CH_3NH_3PbI_3$ [31]) in the radiative limit with and without photon recycling, calculated using the external and internal radiative saturation currents, respectively. We note that the calculated maximum efficiency with photon recycling of 30.2% corroborates previously reported theoretical limits for a similar band-gap $CH_3NH_3PbI_3$ perovskite solar cell [29], where the theoretical J_{SC} ($25.77\ \text{mA cm}^{-2}$) is only slightly higher than what has been achieved experimentally ($25.40\ \text{mA cm}^{-2}$ [48]). These results emphasize the need to optimize V_{OC} and fill factor (FF) through reducing nonradiative recombination and harnessing photon recycling.

TABLE I. *J-V* characteristics and PCE extracted from the simulated *J-V* curve in the radiative limit with and without PR. PR leads primarily to enhancements in the MPP operating voltage (V_{MPP}).

	J_{SC} (mA/cm^2)	V_{OC} (V)	FF	J_{MPP} (mA/cm^2)	V_{MPP} (V)	PCE (%)
No PR	25.77	1.22	0.899	25.19	1.12	28.2
With PR	25.77	1.29	0.906	25.23	1.20	30.2

Table I shows that photon recycling improves PV device performance at both open-circuit and MPP conditions. The V_{OC} increase of $\Delta V_{\text{OC}}^{\text{PR}} = 70\ \text{mV}$ calculated in this work is consistent with the 70 mV value predicted by Kirchartz *et al.* for a planar device architecture with Beer-Lambert absorption [29]. Extending beyond previous studies, our full *J-V* simulation also shows that photon recycling improves the MPP voltage V_{MPP} ($\Delta V_{\text{MPP}}^{\text{PR}} = 80\ \text{mV}$) and the FF, producing an absolute increase in PCE of 2.0%. We note that the short-circuit current density remains unchanged because, with or without photon recycling, J_{SC} only depends on the absorptivity of the material and the solar irradiance.

One highlight of this analysis is that the maximum V_{OC} achievable without photon recycling is only 1.22 V for both the triple-cation and $CH_3NH_3PbI_3$ films (see Supplemental Material Fig. S22 [31])—a voltage deficit of 0.38 V for each formulation. Our results suggest that perovskite PVs (with a band gap of 1.6 eV) exhibiting $V_{\text{OC}} > 1.22\ \text{V}$ and $V_{\text{MPP}} = 1.12\ \text{V}$ benefit from photon recycling [32,36]. In this regard, Liu *et al.* recently reported a record-setting $V_{\text{OC}} = 1.26\ \text{V}$ in $CH_3NH_3PbI_3$ devices, for which our calculations suggest 40 meV can be attributed to photon recycling effects.

B. Incorporating nonradiative recombination

Theoretical photovoltaic performance limits are useful for setting efficiency targets, but most absorber layers perform far from the radiative limit due to nonradiative losses. Perovskites are no exception—typical films exhibit PLQEs of <15% at 1-sun equivalent generation, with k_1 ranging from 10^6 to $10^9\ \text{s}^{-1}$, depending on chemical composition and processing methods [13,16,17]. However, with recently developed passivation techniques, k_1 values have been decreasing and will likely continue to decrease as passivation mechanisms are better understood and implemented. For example, a low nonradiative recombination rate of $k_1 = 1.7 \times 10^5\ \text{s}^{-1}$ has been reported for tri-*n*-octylphosphine oxide (TOPO)-treated $CH_3NH_3PbI_3$ films [18].

To adapt our model to nonidealized scenarios, we modify the saturation current density [Eqs. (3) and (4)] to account for nonradiative Shockley-Read-Hall (SRH) and

Auger recombination, as previously reported by Pazos-Outón *et al.* [Eq. (6)] [29]

$$J_0 = J_0^{\mathrm{rad}} + J_0^{\mathrm{nonrad}} = J_0^{\mathrm{rad}} + J_{\mathrm{SRH}} + J_A, \tag{6}$$

where J_0^{rad} is the radiative recombination rate (external or internal) and J_0^{nonrad} is the sum of the nonradiative, first-order SRH (J_{SRH}) and nonradiative, third-order Auger (J_A) recombination currents. The SRH and Auger recombination rates are described for a carrier density (n) in quasithermal equilibrium using the law of mass action [Eq. (7)]

$$n(V) = n_i e^{qV/2kT}, \tag{7}$$

$$J_{\mathrm{SRH}}(V) = qk_1 n(V)d, \tag{8}$$

$$J_A(V) = qk_3 n^3(V)d, \tag{9}$$

where n_i is the intrinsic carrier density and k_1 and k_3 are the first-order SRH and third-order Auger recombination rate constants, respectively.

Figure 2 shows the impact of different nonradiative recombination values on device performance with and without photon recycling. For these calculations, we use the radiative rate of $k_2^{\mathrm{int}} = 2 \times 10^{-10}\,\mathrm{cm^{-3}\,s^{-1}}$ and the Auger rate of $k_3 = 1 \times 10^{-28}\,\mathrm{cm^6\,s^{-1}}$, which are intrinsic material properties that do not vary significantly with film quality (see Supplemental Material for discussion on model sensitivity to k_2^{int} and k_3 [31]) [17,43]. Figure 2(a) shows the simulated J-V curves with $k_1 = 1 \times 10^4\,\mathrm{s^{-1}}$, which closely resembles those reported in Fig. 1 ($k_1 = 0$), suggesting that radiative recombination outcompetes nonradiative recombination and the benefits of photon recycling are, therefore, observed at this low k_1. Figure 2(b) shows that, as k_1 increases to $2 \times 10^5\,\mathrm{s^{-1}}$, the effect of photon recycling is greatly reduced and eventually becomes negligible when nonradiative rates approach $3 \times 10^6\,\mathrm{s^{-1}}$ [Fig. 2(c)].

Figure 2(d) shows both the V_{OC} and V_{MPP} with and without photon recycling for varying k_1 values. For k_1 exceeding a threshold value of $2 \times 10^6\,\mathrm{s^{-1}}$ (i.e., nonradiative lifetime, $\tau_1 < 500\,\mathrm{ns}$), we observe no increase in V_{OC} and V_{MPP} with photon recycling. For k_1 between $7 \times 10^5\,\mathrm{s^{-1}}$ and $2 \times 10^6\,\mathrm{s^{-1}}$ (i.e., $\tau_1 = 500 - 1430\,\mathrm{ns}$), photon recycling can improve V_{OC}, but the fill-factor decreases, and therefore, PCE enhancements are negligible (see Fig. S9 within the Supplemental Material [31]). With the full J-V simulation, we can see that V_{MPP} is unaffected at these values. Only when k_1 is reduced below $7 \times 10^5\,\mathrm{s^{-1}}$ ($\tau_1 > 1430\,\mathrm{ns}$) does photon recycling improve the MPP and efficiency (Figs. S9 and S10). For example, at $k_1 = 2 \times 10^5\,\mathrm{s^{-1}}$ [Fig. 2(b)], photon recycling increases V_{OC} by 50 mV, but V_{MPP} by only 20 mV (Table II). We note that for $k_1 = 3 \times 10^6\,\mathrm{s^{-1}}$,

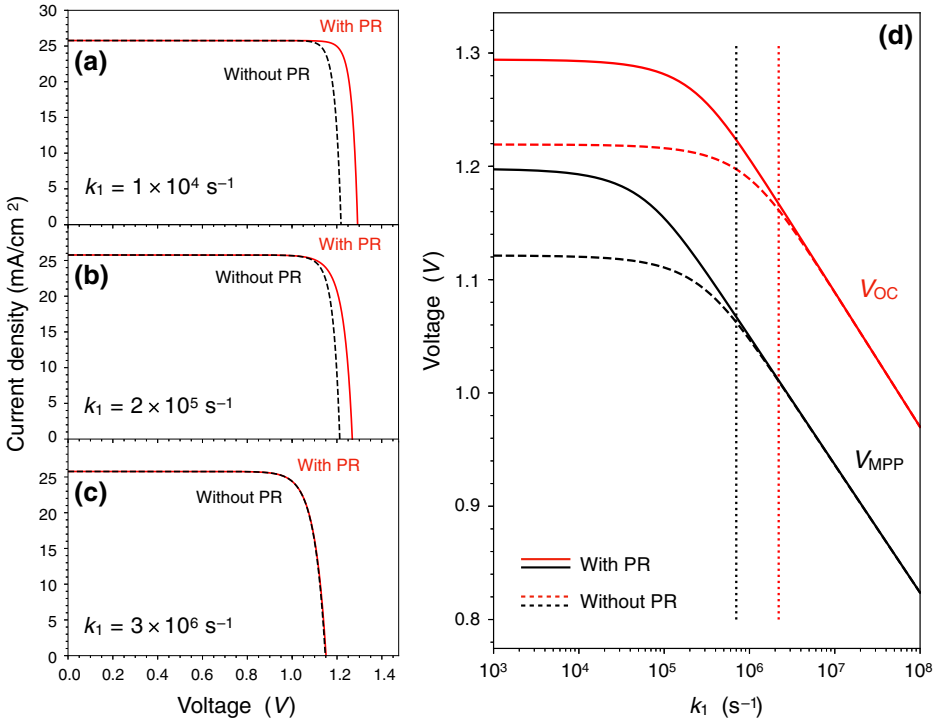

FIG. 2. Simulated J-V curves (triple-cation, 1.6 eV band gap) with and without PR for k_1 values of (a) $1 \times 10^4\,\mathrm{s^{-1}}$, (b) $2 \times 10^5\,\mathrm{s^{-1}}$, and (c) $3 \times 10^6\,\mathrm{s^{-1}}$ ($k_2^{\mathrm{int}} = 2 \times 10^{-10}\,\mathrm{cm^3\,s^{-1}}$ and $k_3 = 1 \times 10^{-28}\,\mathrm{cm^6\,s^{-1}}$). (d) V_{OC} (red lines) and V_{MPP} (black lines) as a function of k_1, revealing differences in the onset of performance improvements due to PR. Dotted vertical red and black lines indicate k_1 thresholds (2×10^6 and $7 \times 10^5\,\mathrm{s^{-1}}$, respectively) below which PR improves performance at open circuit and the MPP, respectively.

TABLE II. Device parameters extracted from the simulated J-V curves for $k_1 = 1 \times 10^4$, 2×10^5, and $3 \times 10^6\ s^{-1}$ ($k_2^{int} = 2 \times 10^{-10}\ cm^3\ s^{-1}$ and $k_3 = 1 \times 10^{-28}\ cm^6\ s^{-1}$) with and without PR.

		J_{SC} (mA/cm^2)	V_{OC} (V)	FF	J_{MPP} (mA/cm^2)	V_{MPP} (V)	PCE (%)
$k_1 = 1\times10^4\ s^{-1}$	No PR	25.77	1.22	0.897	25.13	1.12	28.2
	With PR	25.77	1.29	0.900	25.17	1.19	30.0
$k_1 = 2\times10^5\ s^{-1}$	No PR	25.77	1.21	0.876	24.86	1.10	27.4
	With PR	25.77	1.27	0.850	24.67	1.13	27.8
$k_1 = 3\times10^6\ s^{-1}$	No PR	25.77	1.15	0.824	24.50	1.00	24.4
	With PR	25.77	1.15	0.822	24.50	1.00	24.4

the PCE is comparable to current record-performing devices [49].

C. Competition between radiative and nonradiative recombination currents

To better understand the recombination processes governing PV device behavior with and without photon recycling, we break down the J-V curve from Fig. 2(b) ($k_1 = 2 \times 10^5\ s^{-1}$) into its individual recombination components. The absolute magnitude is calculated using Eqs. (3), (4), (8), and (9), and the fraction of each recombination mechanism is its magnitude divided by the total recombination current (i.e., $J_{SRH,rad,A}/J_{tot}$).

Figures 3(a) and 3(b) show $J_0^{rad,int}$ and $J_0^{rad,ext}$ as a function of voltage, along with J_{SRH} and J_A, which are the SRH and Auger nonradiative pathways, respectively. J_{SRH} and J_A have the same functional form with or without photon recycling, as neither depend on the radiative saturation current [Eqs. (8) and (9)]. Photon recycling requires the

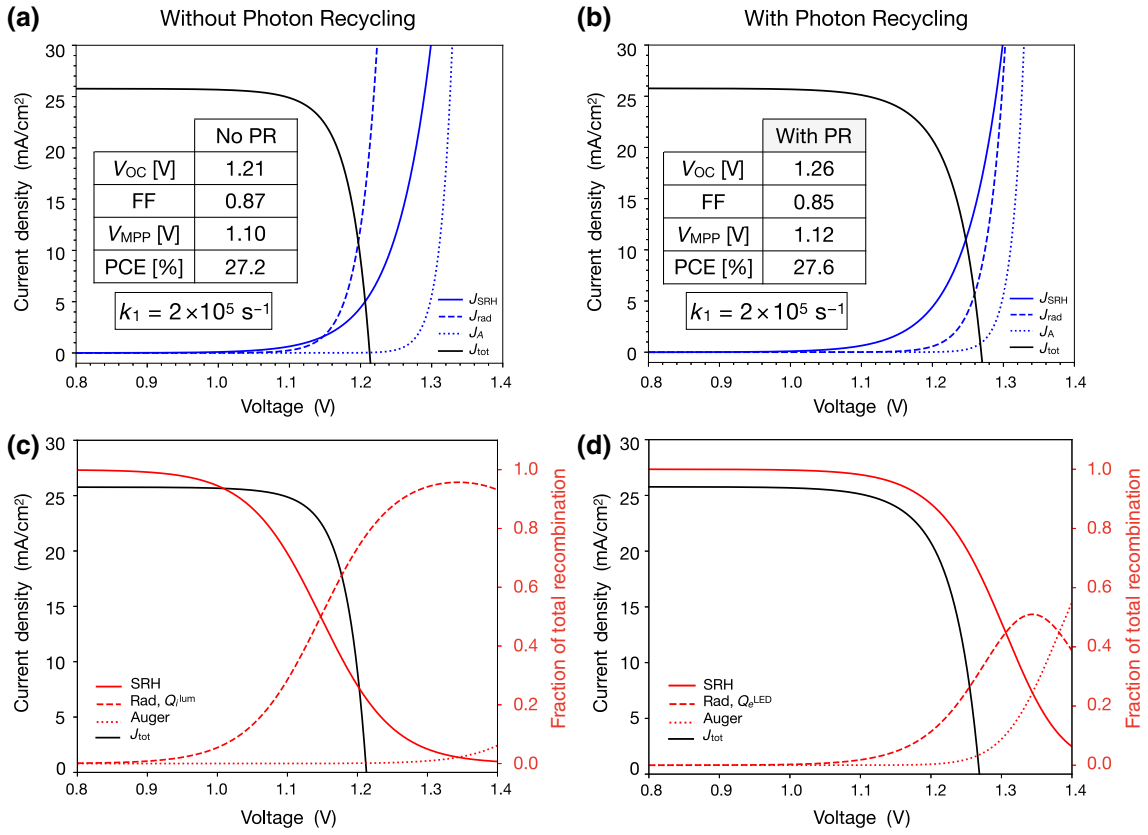

FIG. 3. Simulated J-V curves (black traces) for $k_1 = 2 \times 10^5\ s^{-1}$, $k_2^{int} = 2 \times 10^{-10}\ cm^3\ s^{-1}$, and $k_3 = 1 \times 10^{-28}\ cm^6\ s^{-1}$ (a),(c) without and (b),(d) with PR are shown with the magnitude of SRH, radiative, and Auger recombination currents as a function of voltage (blue traces). (c),(d) The fractions of total recombination current due to SRH, radiative, and Auger recombination are shown at each voltage (red traces) (c) without and (d) with PR. The fraction of radiative recombination as a function of voltage with and without PR is equivalent to Q_e^{LED} and Q_i^{lum}, respectively.

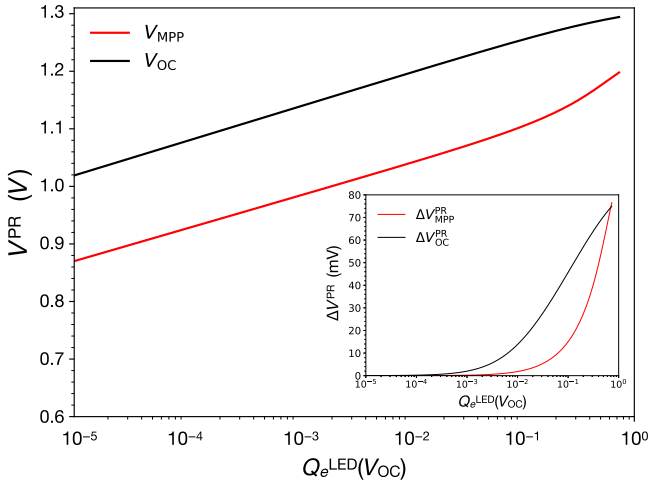

FIG. 4. The voltage with PR (V^{PR}) for $P_{esc} = 4.7\%$ at the MPP and open circuit is shown as a function of $Q_e^{LED}(V_{OC})$, which, as nonradiative recombination decreases, approaches unity. Inset: ΔV^{PR} for $P_{esc} = 4.7\%$ at MPP and open circuit as a function of $Q_e^{LED}(V_{OC})$.

reabsorption of emitted photons; if the recombination process is nonradiative (i.e., SRH, Auger), no photons are generated for the reabsorption process. We observe that photon recycling shifts radiative recombination to higher onset voltages, and therefore, reduces the magnitude of the radiative saturation current at MPP, leading to increases in V_{OC} and V_{MPP} with photon recycling (Table II, $k_1 = 2 \times 10^5\ s^{-1}$). Figures 3(c) and 3(d) give further insight into these results, where the fractions of each recombination current are compared as a function of voltage. With photon recycling, SRH recombination becomes the limiting pathway (solid blue and red traces). To harness photon recycling in devices, it is essential to reduce nonradiative recombination pathways through improved processing or passivation techniques. For example, alkali metal salt additives and interfacial passivation layers have yielded low voltage-deficit devices (e.g., <0.35 V), which we predict currently benefit from, but do not fully harness, photon recycling [36,50].

We note that the radiative recombination fraction without photon recycling in Fig. 3(c) is equal to the internal luminescence quantum efficiency (Q_i^{lum}), which has similarly been defined elsewhere [38]

$$Q_i^{lum}(V) = \frac{J_0^{rad,int}(V)}{J_{SRH}(V) + J_0^{rad,int}(V) + J_A(V)}. \tag{10}$$

The radiative recombination fraction with photon recycling in Fig. 3(d) yields the external light-emitting diode (LED) electroluminescence efficiency (Q_e^{LED}), which is connected to the mean probability of photon escape from the film (P_{esc}) through a geometric series [38]

$$Q_e^{LED}(V) = \frac{P_{esc} Q_i^{lum}(V)}{1 - Q_i^{lum}(V)(1 - P_{esc})}. \tag{11}$$

Here, the escape probability (P_{esc}) can be defined as the ratio of the external to the internal radiative saturation current [38]

$$P_{esc} = \frac{J_0^{rad,ext}}{J_0^{rad,int}}. \tag{12}$$

III. EXTERNAL ELECTROLUMINESCENCE EFFICIENCY ENHANCEMENTS

Q_e^{LED} is a function of the injection current, and thus it is necessary to denote both the injection current and corresponding voltage at which the current is achieved for a

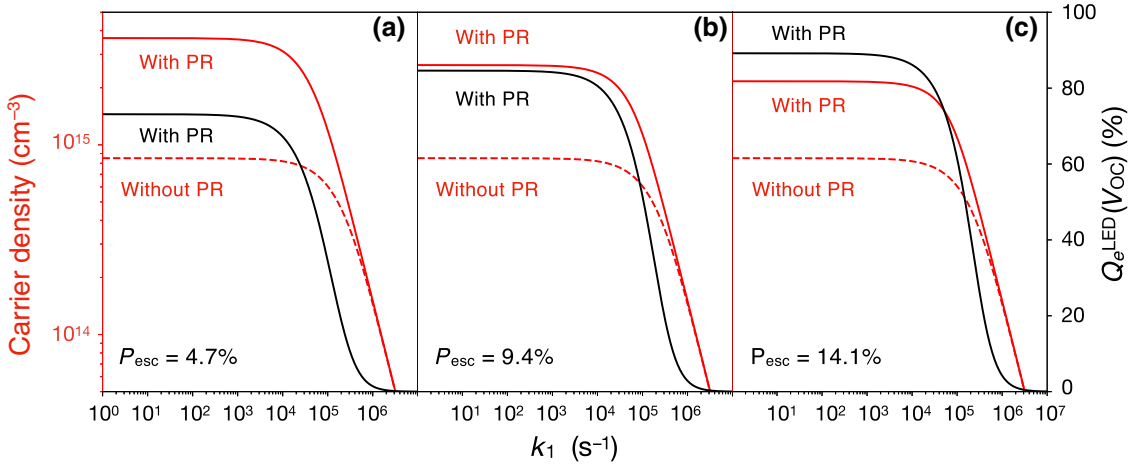

FIG. 5. The effect of PR on the MPP steady-state carrier density and $Q_e^{LED}(V_{OC})$ as a function of k_1 for (a) $P_{esc} = 4.7\%$, (b) 9.4%, and (c) 14.1%.

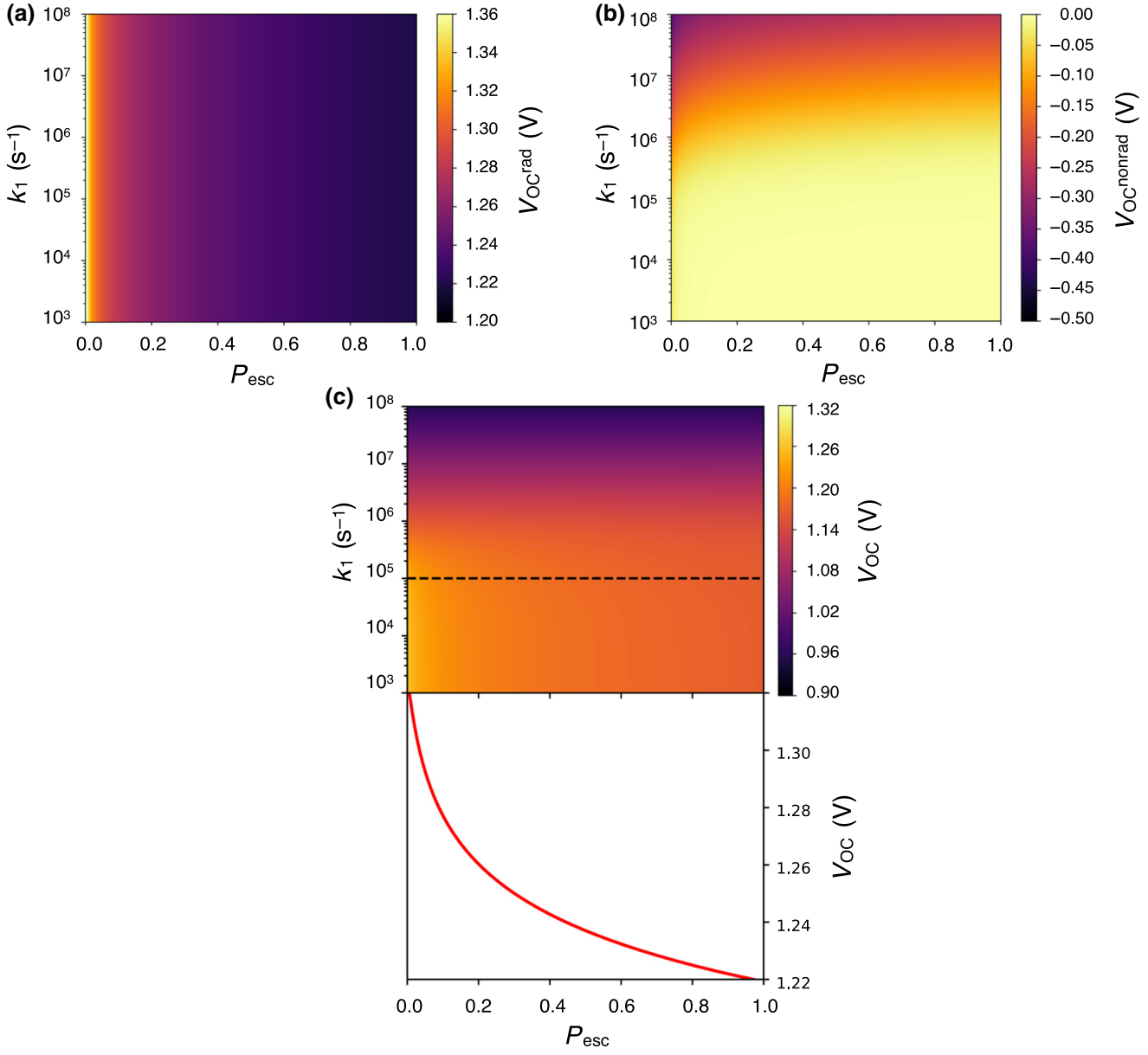

FIG. 6. (a) The V_{OC} with PR in the radiative limit (V_{OC}^{rad}) is shown along with (b) the nonradiative subtractive effect on V_{OC}^{max} (V_{OC}^{nonrad}). Combined, $V_{OC}^{rad} + V_{OC}^{nonrad}$ yield (c) the total V_{OC}^{max} as a function of k_1 and P_{esc}, with a dashed line at $k_1 = 1 \times 10^5\ s^{-1}$ showing that increasing P_{esc} for a fixed Q_i^{lum} decreases V_{OC}.

given Q_e^{LED}. Due to the reciprocity relations that link optical output to electrical input, Q_e^{LED} values are often measured at an injection current equivalent to the photocurrent [51,52]. Unless otherwise stated, we report Q_e^{LED} values calculated with an injection current equivalent to J_{SC} – that is, applied voltage equal to V_{OC}, $Q_e^{LED}(V_{OC})$. Considering Eq. (11), Fig. 3(d) shows that a device with $k_1 = 2 \times 10^5\ s^{-1}$(i.e., $\tau_1 = 5\,\mu s$) should demonstrate a $Q_e^{LED}(V_{OC})$ of 31.5%. Importantly, the external emission efficiency of a solar cell is a metric that has been shown to directly correlate with power conversion efficiency, and therefore, serves as a useful optimization parameter [53,54]. Eqs. (9) and (10) provide two apparent routes: decreasing J_{SRH} and J_A and/or increasing P_{esc} to increase $Q_e^{LED}(V_{OC})$. To evaluate which method best capitalizes on the benefits of photon recycling, we examine the dependence of $Q_e^{LED}(V_{OC})$ and P_{esc} on V_{OC} and V_{MPP}.

A. Modification of nonradiative recombination

First, we consider how $Q_e^{LED}(V_{OC})$ and photovoltage are affected by decreasing J_{SRH} [i.e., varying k_1 in Eq. (8)], for a fixed escape probability ($P_{esc} = 4.7\%$). Figure 4 shows $Q_e^{LED}(V_{OC})$ increases with decreasing

k_1, resulting in voltage enhancements at open circuit and MPP. We report a photon recycling threshold of $Q_e^{\mathrm{LED}}(V_{\mathrm{OC}}) >\sim 0.3\%$ and significant performance improvements for $Q_e^{\mathrm{LED}}(V_{\mathrm{OC}}) = 10\%$, yielding $\Delta V_{\mathrm{OC}}^{\mathrm{PR}} = 36\,\mathrm{mV}$ and $\Delta V_{\mathrm{MPP}}^{\mathrm{PR}} = 9\,\mathrm{mV}$ (Fig. 4). Recently, Liu *et al.* reported a $Q_e^{\mathrm{LED}}(V_{\mathrm{OC}})$ of $7.5 \pm 2.5\%$ for $CH_3NH_3PbI_3$ devices achieving a V_{OC} of 1.26 V. This experimental V_{OC} is higher than the maximum achievable theoretical V_{OC} in the radiative limit without photon recycling, indicating performance enhancements due to photon recycling [36].

B. Modification of probability of photon escape

Second, we consider how $Q_e^{\mathrm{LED}}(V_{\mathrm{OC}})$ and photovoltage (see below) are affected by increasing P_{esc} and decreasing k_1. We note that the photovoltage is proportional to the steady-state carrier density and is, therefore, an intuitive metric to compare across the multiple varying parameters. We calculate the carrier density using the law of mass action [Eq. (7)] as a function of k_1 and P_{esc}.

Figure 5(a) shows that at $P_{\mathrm{esc}} = 4.7\%$ and low k_1 values, photon recycling increases the steady-state carrier density by a factor of four, from 8.5×10^{14} to $3.7 \times 10^{15}\,\mathrm{cm}^{-3}$ at MPP. This high carrier density results from additional generation associated with the reabsorption of trapped photons—up to 18-suns equivalent at open circuit and >1.4 equivalent suns at MPP (see Figs. S12 and S13 for triple-cation and Fig. S27 for $CH_3NH_3PbI_3$within the Supplemental Material [31]). Figure 5 shows that photon recycling allows $Q_e^{\mathrm{LED}}(V_{\mathrm{OC}})$ to exceed the escape probability (see Figs. S14 and S15 within the Supplemental Material [31]), a direct result from the multiple reabsorption events that rerandomize the photon propagation angle. While the emission efficiency can increase beyond P_{esc} as nonradiative recombination decreases, $Q_e^{\mathrm{LED}}(V_{\mathrm{OC}})$ cannot reach 100% due to the higher fraction of Auger recombination at increased steady-state carrier densities, as shown in Figs. 3(c) and 3(d). A similar limiting effect for the efficiency droop at high applied voltages in GaN LEDs has been attributed to Auger recombination processes [55,56].

Next, we consider scenarios in which P_{esc} is changed without significantly impacting the material absorptivity function (see Supplemental Material for model assumptions [31]). Figures 5(b) and 5(c) show the carrier density and $Q_e^{\mathrm{LED}}(V_{\mathrm{OC}})$ for $P_{\mathrm{esc}} = 9.4\%$ and 14.1%. Here, the steady-state carrier density steadily decreases, while $Q_e^{\mathrm{LED}}(V_{\mathrm{OC}})$ approaches 90% with photon recycling due to a smaller contribution from Auger recombination at lower carrier densities. These results appear to counteract one another, as both a high steady-state carrier density and high $Q_e^{\mathrm{LED}}(V_{\mathrm{OC}})$ are desired.

This observation raises the question as to whether solely increasing the escape probability can enhance device performance and, in particular, open-circuit voltage [15,16]. The traditional definition of the maximum achievable open-circuit voltage ($V_{\mathrm{OC}}^{\mathrm{max}}$) is expressed as a function of the external LED electroluminescence efficiency, as described in Eq. (13) [38,51,57].

$$V_{\mathrm{OC}}^{\mathrm{max}} = V_{\mathrm{OC}}^{\mathrm{rad}} + \frac{kT}{q} \ln\left[Q_e^{\mathrm{LED}}(V_{\mathrm{OC}})\right]. \tag{13}$$

Here, it appears that increasing $Q_e^{\mathrm{LED}}(V_{\mathrm{OC}})$ through enhancing the escape probability should allow $V_{\mathrm{OC}}^{\mathrm{max}}$ to approach $V_{\mathrm{OC}}^{\mathrm{rad}}$—however, the implicit dependence of the radiative component ($V_{\mathrm{OC}}^{\mathrm{rad}}$) on P_{esc} is often overlooked. This dependence becomes clear if we equate $J_0^{\mathrm{rad,ext}}$ with the product of $J_0^{\mathrm{rad,int}}$ and P_{esc} [Eq. (14)], where it can be seen that this term decreases as the escape probability increases [58].

$$V_{\mathrm{OC}}^{\mathrm{rad}} = \frac{kT}{q} \ln\left[\frac{J_{\mathrm{SC}}}{J_0^{\mathrm{rad,ext}}}\right] = \frac{kT}{q} \ln\left[\frac{J_{\mathrm{SC}}}{P_{\mathrm{esc}} J_0^{\mathrm{rad,int}}}\right]. \tag{14}$$

IV. EFFECT OF NONRADIATIVE RECOMBINATION AND PROBABILITY OF ESCAPE ON V_{OC}

To better understand the competition between $V_{\mathrm{OC}}^{\mathrm{rad}}$ and $Q_e^{\mathrm{LED}}(V_{\mathrm{OC}})$ on $V_{\mathrm{OC}}^{\mathrm{max}}$, Figs. 6(a) and 6(b) show the magnitude of these terms as a function of P_{esc} and k_1. As P_{esc} increases for a given k_1, $V_{\mathrm{OC}}^{\mathrm{rad}}$ decreases due to the enhanced light outcoupling, which increases the external radiative saturation current. Opposing this negative impact on $V_{\mathrm{OC}}^{\mathrm{max}}$ from $V_{\mathrm{OC}}^{\mathrm{rad}}$, $V_{\mathrm{OC}}^{\mathrm{nonrad}}$ also decreases with increasing P_{esc}, resulting in a smaller subtractive component from $V_{\mathrm{OC}}^{\mathrm{max}}$, as shown in Fig. 6(b). As P_{esc} changes, the radiative and nonradiative terms vary in opposing directions.

Ultimately, $V_{\mathrm{OC}}^{\mathrm{max}}$ is dominated by the radiative dependence on P_{esc}, so $V_{\mathrm{OC}}^{\mathrm{max}}$ decreases monotonically with increasing P_{esc} at a constant k_1 value [Fig. 6(c)] [16]. Thus, it is evident that simply increasing the outcoupling efficiency reduces output voltages due to the reduction in steady-state carrier density (cf. Fig. 5). We highlight that we only analyze the voltage in this simulation, and note that overall device performance may not track the changes in voltage if, for example, J_{SC} also changes.

V. CONCLUSION

In summary, we present a rigorous method for evaluating the extent of and benefits from photon recycling in emerging perovskite absorbers by exploring device performance limits using experimentally determined optical constants and absorption for triple-cation films. This analysis investigates the effect of photon recycling on both V_{OC} and operationally relevant MPP parameters, both in the radiative limit and with nonradiative recombination. Our simulations provide a framework for evaluating the

improvements attributable to photon recycling in standard current-voltage measurements. This analysis reveals that perovskite devices demonstrating voltage deficits of <0.38 V [32,36] already benefit from photon recycling. This would mean that high-quality devices fabricated today may be further improved by reducing nonradiative recombination and/or modifying the escape probability to harness the benefits of photon recycling.

With recycling, photons waveguided within the film can be reabsorbed and reemitted in the escape cone, allowing $Q_e^{\mathrm{LED}}(V_{\mathrm{OC}})$ to approach the intrinsic limit while maintaining a high steady-state carrier density. If $Q_e^{\mathrm{LED}}(V_{\mathrm{OC}})$ is enhanced only by increasing P_{esc}, the steady-state carrier density will decrease, resulting in a lower V_{OC}. For triple-cation films, enhancements in V_{OC} and V_{MPP} are observed for $k_1 < 2 \times 10^6\ \mathrm{s}^{-1}$ ($\tau_1 > 500\ \mathrm{ns}$) and $k_1 < 7 \times 10^5\ \mathrm{s}^{-1}$ ($\tau_1 > 1430\ \mathrm{ns}$), respectively, while, for $k_1 < 1 \times 10^4\ \mathrm{s}^{-1}$ ($\tau_1 > 100\ \mu\mathrm{s}$), further performance improvements become negligible. Our analysis, therefore, identifies a target nonradiative recombination rate for perovskite films of $k_1 < 1 \times 10^4\ \mathrm{s}^{-1}$. Below this threshold, the steady-state carrier density plateaus at 4× the density without photon recycling. In theory, a perovskite film reaching this lower bound of $k_1 = 1 \times 10^4\ \mathrm{s}^{-1}$ ($P_{\mathrm{esc}} = 4.7\%$) can achieve a 74 mV increase in V_{OC}, 73 mV improvement in V_{MPP}, 0.3% absolute increase in FF, and 1.79% increase in PCE—due solely to photon recycling.

We note that the model used to simulate *J-V* curves in this study represents an ideal case and sets an upper limit for the target nonradiative recombination rate constants. For example, perovskite material quality will likely need to be even better than these targets, as charge transport layers in devices introduce new pathways for interfacial recombination. Passivation methods and surface modifiers that reduce the number of defects at the interfaces and lead to favorable band alignment will be critical in minimizing nonradiative loss to fully harness photon recycling [18,24,25]. Toward the development of improved perovskite formulations and device architectures, this analysis provides clear material quality targets and device performance limits for evaluating photon recycling in next-generation perovskite solar cells.

ACKNOWLEDGMENTS

This work is supported by the TATA-MIT GridEdge Solar Research program. This material is based upon work supported by the National Science Foundation Graduate Research Fellowship under Grant No. (1122374). We would also like to acknowledge support from NSF/CBET-BSF under Grant No. 1605406 (EP/L000202). We thank Dak Benjia Dou for his guidance in the preparation of the triple-cation perovskite thin films; Nina Hong, from J.A. Woollam Co., Inc., for her technical support analyzing the ellipsometry data; and Luis Pazos-Outón and Thomas Mahony for valuable discussions.

[1] E. Yablonovitch, Lead halides join the top optoelectronic league, Science **351**, 1401 (2016).
[2] O. D. Miller and E. Yablonovitch, Photon extraction: The key physics for approaching solar cell efficiency limits, Proc. SPIE **8808**, 880807 (2013).
[3] O. D. Miller, E. Yablonovitch, and S. R. Kurtz, Strong internal and external luminescence as solar cells approach the Shockley-Queisser limit, IEEE J. Photovoltaics **2**, 303 (2012).
[4] M. A. Steiner, J. F. Geisz, I. García, D. J. Friedman, A. Duda, and S. R. Kurtz, Optical enhancement of the open-circuit voltage in high quality GaAs solar cells, J. Appl. Phys. **113**, 123109 (2013).
[5] R. K. Ahrenkiel, D. J. Dunlavy, B. Keyes, S. M. Vernon, T. M. Dixon, S. P. Tobin, K. L. Miller, and R. E. Hayes, Ultralong minority-carrier lifetime epitaxial GaAs by photon recycling, Appl. Phys. Lett. **55**, 1088 (1989).
[6] A. W. Walker, O. Höhn, D. N. Micha, B. Bläsi, A. W. Bett, and F. Dimroth, Impact of photon recycling on GaAs solar cell designs, IEEE J. Photovoltaics **5**, 1636 (2015).
[7] A. Braun, E. A. Katz, D. Feuermann, B. M. Kayes, and J. M. Gordon, Photovoltaic performance enhancement by external recycling of photon emission, Energy Environ. Sci. **6**, 1499 (2013).
[8] F. Staub, H. Hempel, J.-C. Hebig, J. Mock, U. W. Paetzold, U. Rau, T. Unold, and T. Kirchartz, Beyond Bulk Lifetimes: Insights into Lead Halide Perovskite Films from Time-Resolved Photoluminescence, Phys. Rev. Appl. **6**, 044017 (2016).
[9] F. Staub, T. Kirchartz, K. Bittkau, and U. Rau, Manipulating the net radiative recombination rate in lead halide perovskite films by modification of light outcoupling, J. Phys. Chem. Lett. **8**, 5084 (2017).
[10] R. K. Ahrenkiel, B. M. Keyes, G. B. Lush, M. R. Melloch, M. S. Lundstrom, and H. F. MacMillan, Minority-carrier lifetime and photon recycling in *n*-GaAs, J. Vac. Sci. Technol. A **10**, 990 (1992).
[11] J. L. Balenzategui and A. Martí, Detailed modelling of photon recycling: Application to GaAs solar cells, Sol. Energy Mater. Sol. Cells **90**, 1068 (2006).
[12] P. Renaud, F. Raymond, B. Bensaïd, and C. Vèrié, Influence of photon recycling on lifetime and diffusion coefficient in GaAs, J. Appl. Phys. **71**, 1907 (1992).
[13] L. M. Pazos-Outon, M. Szumilo, R. Lamboll, J. M. Richter, M. Crespo-Quesada, M. Abdi-Jalebi, H. J. Beeson, M. Vru ini, M. Alsari, H. J. Snaith, B. Ehrler, R. H. Friend, and F. Deschler, Photon recycling in lead iodide perovskite solar cells, Science **351**, 1430 (2016).
[14] Y. Fang, H. Wei, Q. Dong, and J. Huang, Quantification of re-absorption and re-emission processes to determine photon recycling efficiency in perovskite single crystals, Nat. Commun. **8**, 14417 (2017).
[15] W. Tress, Perovskite solar cells on the way to their radiative efficiency limit – Insights into a success story of high

open-circuit voltage and low recombination, Adv. Energy Mater. **7**, 1602358 (2017).

[16] J. M. Richter, M. Abdi-Jalebi, A. Sadhanala, M. Tabachnyk, J. P. H. Rivett, L. M. Pazos-Outón, K. C. Gödel, M. Price, F. Deschler, and R. H. Friend, Enhancing photoluminescence yields in lead halide perovskites by photon recycling and light out-coupling, Nat. Commun. **7**, 13941 (2016).

[17] M. B. Johnston and L. M. Herz, Hybrid perovskites for photovoltaics: Charge-carrier recombination, diffusion, and radiative efficiencies, Acc. Chem. Res. **49**, 146 (2016).

[18] I. Braly, D. W. deQuilettes, L. M. Pazos-Outón, S. Burke, M. E. Ziffer, D. S. Ginger, and H. W. Hillhouse, Hybrid perovskite films approaching the radiative limit with over 90% internal photoluminescence quantum efficiency, Nat. Photonics **12**, 355 (2018).

[19] Q. Dong, Y. Fang, Y. Shao, P. Mulligan, J. Qiu, L. Cao, and J. Huang, Electron-hole diffusion lengths > 175 μm in solution-grown $CH_3NH_3PbI_3$ single crystals, Science **347**, 967 (2015).

[20] Y. Fang, Q. Dong, Y. Shao, Y. Yuan, and J. Huang, Highly narrowband perovskite single-crystal photodetectors enabled by surface-charge recombination, Nat. Photonics **9**, 679 (2015).

[21] Y. Yamada, T. Yamada, and Y. Kanemitsu, Free carrier radiative recombination and photon recycling in lead halide perovskite solar cell materials, Bull. Chem. Soc. Jpn **90**, 1129 (2017).

[22] T. Yamada, Y. Yamada, Y. Nakaike, A. Wakamiya, and Y. Kanemitsu, Photon Emission and Reabsorption Processes in $CH_3NH_3PbBr_3$ Single Crystals Revealed by Time-Resolved Two-Photon-Excitation Photoluminescence Microscopy, Phys. Rev. Appl. **7**, 014001 (2017).

[23] Y. Kanemitsu, Luminescence spectroscopy of lead-halide perovskites: materials properties and application as photovoltaic devices, J. Mater. Chem. C **5**, 3427 (2017).

[24] R. Brenes, D. Guo, A. Osherov, N. K. Noel, C. Eames, E. M. Hutter, S. K. Pathak, F. Niroui, R. H. Friend, M. S. Islam, H. J. Snaith, V. Bulović, T. J. Savenije, and S. D. Stranks, Metal halide perovskite polycrystalline films exhibiting properties of single crystals, Joule **1**, 155 (2017).

[25] M. Abdi-Jalebi, Z. Andaji-Garmaroudi, S. Cacovich, C. Stavrakas, B. Philippe, J. M. Richter, M. Alsari, E. P. Booker, E. M. Hutter, A. J. Pearson, S. Lilliu, T. J. Savenije, H. Rensmo, G. Divitini, C. Ducati, R. H. Friend, and S. D. Stranks, Maximizing and stabilizing luminescence from halide perovskites with potassium passivation, Nature **555**, 497 (2018).

[26] I. Schnitzer, E. Yablonovitch, C. Caneau, and T. J. Gmitter, Ultrahigh spontaneous emission quantum efficiency, 99.7% internally and 72% externally, from AlGaAs/GaAs/AlGaAs double heterostructures, Appl. Phys. Lett. **62**, 131 (1993).

[27] M. Saliba, T. Matsui, J.-Y. Seo, K. Domanski, J.-P. Correa-Baena, M. K. Nazeeruddin, S. M. Zakeeruddin, W. Tress, A. Abate, A. Hagfeldt, and M. Grätzel, Cesium-containing triple cation perovskite solar cells: Improved stability, reproducibility and high efficiency, Energy Environ. Sci. **9**, 1989 (2016).

[28] J. A. Christians, P. Schulz, J. S. Tinkham, T. H. Schloemer, S. P. Harvey, B. J. Tremolet de Villers, A. Sellinger, J. J. Berry, and J. M. Luther, Tailored interfaces of unencapsulated perovskite solar cells for $>$1,000 hour operational stability, Nat. Energy **3**, 68 (2018).

[29] L. M. Pazos-Outón, T. P. Xiao, and E. Yablonovitch, Fundamental efficiency limit of lead iodide perovskite solar cells1, J. Phys. Chem. Lett. **9**, 1703 (2018).

[30] S. M. Durbin and J. L. Gray, Numerical modeling of photon recycling in solar cells, IEEE Trans. Electron Devices **41**, 239 (1994).

[31] See Supplemental Material at http://link.aps.org/supplemental/10.1103/PhysRevApplied.12.014017 for full experimental methods, model assumptions, absorption spectra and extension of the analysis for $CH_3NH_3PbI_3$ films, (n.d.).

[32] S. Gholipour and M. Saliba, From exceptional properties to stability challenges of perovskite solar cells, Small **14**, 1802385 (2018).

[33] M. Saliba, T. Matsui, K. Domanski, J.-Y. Seo, A. Ummadisingu, S. M. Zakeeruddin, J.-P. Correa-Baena, W. R. Tress, A. Abate, A. Hagfeldt, and M. Gratzel, Incorporation of rubidium cations into perovskite solar cells improves photovoltaic performance, Science **354**, 206 (2016).

[34] M. Saliba, J. P. Correa-Baena, C. M. Wolff, M. Stolterfoht, N. Phung, S. Albrecht, D. Neher, and A. Abate, How to make over 20% efficient perovskite solar cells in regular (n-i-p) and inverted (p-i-n) architectures, Chem. Mater. **30**, 4193 (2018).

[35] W. Tress, M. Yavari, K. Domanski, P. Yadav, B. Niesen, J. P. Correa Baena, A. Hagfeldt, and M. Graetzel, Interpretation and evolution of open-circuit voltage, recombination, ideality factor and subgap defect states during reversible light-soaking and irreversible degradation of perovskite solar cells, Energy Environ. Sci. **11**, 151 (2018).

[36] Z. Liu, L. Krückemeier, B. Krogmeier, B. Klingebiel, J. A. Márquez, S. Levcenko, S. Öz, S. Mathur, U. Rau, T. Unold, and T. Kirchartz, Open-circuit voltages exceeding 1.26 V in planar methylammonium lead iodide perovskite solar cells, ACS Energy Lett. **4**, 110 (2019).

[37] T. Kirchartz, F. Staub, and U. Rau, Impact of photon recycling on the open-circuit voltage of metal halide perovskite solar cells, ACS Energy Lett. **1**, 731 (2016).

[38] U. Rau, U. W. Paetzold, and T. Kirchartz, Thermodynamics of light management in photovoltaic devices, Phys. Rev. B **90**, 035211 (2014).

[39] A. Martí, J. L. Balenzategui, and R. F. Reyna, Photon recycling and Shockley's diode equation, J. Appl. Phys. **82**, 4067 (1997).

[40] J. K. Katahara and H. W. Hillhouse, Quasi-Fermi level splitting and sub-bandgap absorptivity from semiconductor photoluminescence, J. Appl. Phys. **116**, 173504 (2014).

[41] J. Bisquert, *The Physics of Solar Cells, Taylor & Francis Group* (CRC Press, Boca Raton, FL, 2018).

[42] W. van Roosbroeck and W. Shockley, Photon-radiative recombination of electrons and holes in Germanium, Phys. Rev. **94**, 1558 (1954).

[43] A. Kumar, A. Priyadarshi, S. Shukla, M. Manjappa, L. J. Haur, S. G. Mhaisalkar, and R. Singh, Ultrafast THz photophysics of solvent engineered triple-cation halide perovskites, J. Appl. Phys. **124**, 215106 (2018).

[44] A. Mahboubi Soufiani, Z. Yang, T. Young, A. Miyata, A. Surrente, A. Pascoe, K. Galkowski, M. Abdi-Jalebi, R. Brenes, J. Urban, N. Zhang, V. Bulović, O. Portugall, Y.-B. Cheng, R. J. Nicholas, A. Ho-Baillie, M. A. Green, P. Plochocka, and S. D. Stranks, Impact of microstructure on the electron–hole interaction in lead halide perovskites, Energy Environ. Sci. **10**, 1358 (2017).

[45] T. W. Crothers, R. L. Milot, J. B. Patel, E. S. Parrott, J. Schlipf, P. Müller-Buschbaum, M. B. Johnston, and L. M. Herz, Photon reabsorption masks intrinsic bimolecular charge-carrier recombination in $CH_3NH_3PbI_3$ perovskite, Nano Lett. **17**, 5782 (2017).

[46] A. D. Wright, R. L. Milot, G. E. Eperon, H. J. Snaith, M. B. Johnston, and L. M. Herz, Band-tail recombination in hybrid lead iodide perovskite, Adv. Funct. Mater. **27**, 1700860 (2017).

[47] J. Mattheis, U. Rau, and J. H. Werner, Light absorption and emission in semiconductors with band gap fluctuations—A study on Cu(In, Ga)Se_2 thin films, J. Appl. Phys. **101**, 113519 (2007).

[48] M. A. Green, Y. Hishikawa, E. D. Dunlop, D. H. Levi, J. Hohl-Ebinger, M. Yoshita, and A. W. Y. Ho-Baillie, Solar cell efficiency tables (Version 53), Prog. Photovoltaics Res. Appl. **27**, 3 (2019).

[49] National Renewable Enery Laboratory, *Perovskite efficiency chart*, (NREL, Lakewood, 2018).

[50] S. Yang, J. Dai, Z. Yu, Y. Shao, Y. Zhou, X. Xiao, X. C. Zeng, and J. Huang, Tailoring passivation molecular structures for extremely small open-circuit voltage loss in perovskite solar cells, J. Am. Chem. Soc. **141**, 5781 (2019).

[51] U. Rau, Reciprocity relation between photovoltaic quantum efficiency and electroluminescent emission of solar cells, Phys. Rev. B **76**, 085303 (2007).

[52] W. Tress, N. Marinova, O. Inganäs, M. K. Nazeeruddin, S. M. Zakeeruddin, and M. Graetzel, Predicting the open-circuit voltage of $CH_3NH_3PbI_3$ perovskite solar cells using electroluminescence and photovoltaic quantum efficiency spectra: The role of radiative and non-radiative recombination, Adv. Energy Mater. **5**, 1400812 (2015).

[53] M. A. Green and S. P. Bremner, Energy conversion approaches and materials for high-efficiency photovoltaics, Nat. Mater. **16**, 23 (2017).

[54] M. A. Green, Radiative efficiency of state-of-the-art photovoltaic cells, Prog. Photovoltaics Res. Appl. **20**, 472 (2012).

[55] J. Iveland, L. Martinelli, J. Peretti, J. S. Speck, and C. Weisbuch, Direct Measurement of Auger Electrons Emitted from a Semiconductor Light-Emitting Diode under Electrical Injection: Identification of the Dominant Mechanism for Efficiency Droop, Phys. Rev. Lett. **110**, 177406 (2013).

[56] E. Kioupakis, P. Rinke, K. T. Delaney, and C. G. Van de Walle, Indirect Auger recombination as a cause of efficiency droop in nitride light-emitting diodes, Appl. Phys. Lett. **98**, 161107 (2011).

[57] R. T. Ross, Some Thermodynamics of Photochemical Systems, J. Chem. Phys. **46**, 4590 (1967).

[58] M. G. Abebe, A. Abass, G. Gomard, L. Zschiedrich, U. Lemmer, B. S. Richards, C. Rockstuhl, and U. W. Paetzold, Rigorous treatment of photon recycling in thermodynamics of photovoltaics: The case of perovskite thin-film solar cells, Phys. Rev. B **98**, 075141 (2018).